AIP | Physics of Plasmas

Improving cryogenic deuterium–tritium implosion performance on OMEGA

T. C. Sangster, V. N. Goncharov, R. Betti, P. B. Radha, T. R. Boehly et al.

Citation: Phys. Plasmas **20**, 056317 (2013); doi: 10.1063/1.4805088
View online: http://dx.doi.org/10.1063/1.4805088
View Table of Contents: http://pop.aip.org/resource/1/PHPAEN/v20/i5
Published by the American Institute of Physics.

Improving cryogenic deuterium–tritium implosion performance on OMEGA[a)]

T. C. Sangster,[1,b)] V. N. Goncharov,[1,c)] R. Betti,[1,c),d)] P. B. Radha,[1] T. R. Boehly,[1] D. T. Casey,[2,e)] T. J. B. Collins,[1] R. S. Craxton,[1] J. A. Delettrez,[1] D. H. Edgell,[1] R. Epstein,[1] C. J. Forrest,[1] J. A. Frenje,[2] D. H. Froula,[1] M. Gatu-Johnson,[2] Y. Yu. Glebov,[1] D. R. Harding,[1,f)] M. Hohenberger,[1] S. X. Hu,[1] I. V. Igumenshchev,[1] R. Janezic,[1] J. H. Kelly,[1] T. J. Kessler,[1] C. Kingsley,[1] T. Z. Kosc,[1] J. P. Knauer,[1] S. J. Loucks,[1] J. A. Marozas,[1] F. J. Marshall,[1] A. V. Maximov,[1] R. L. McCrory,[1,c),d)] P. W. McKenty,[1] D. D. Meyerhofer,[1,c),d)] D. T. Michel,[1] J. F. Myatt,[1] R. D. Petrasso,[2] S. P. Regan,[1] W. Seka,[1] W. T. Shmayda,[1] R. W. Short,[1] A. Shvydky,[1] S. Skupsky,[1] J. M. Soures,[1] C. Stoeckl,[1] W. Theobald,[1] V. Versteeg,[1] B. Yaakobi,[1] and J. D. Zuegel[1]

[1]*Laboratory for Laser Energetics, University of Rochester, 250 East River Road, Rochester, New York 14623, USA*

[2]*Massachusetts Institute for Technology, Plasma Science and Fusion Center, Cambridge, Massachusetts 02139, USA*

(Received 12 December 2012; accepted 19 April 2013; published online 28 May 2013)

A flexible direct-drive target platform is used to implode cryogenic deuterium–tritium (DT) capsules on the OMEGA laser [Boehly *et al.*, Opt. Commun. **133**, 495 (1997)]. The goal of these experiments is to demonstrate ignition hydrodynamically equivalent performance where the laser drive intensity, the implosion velocity, the fuel adiabat, and the in-flight aspect ratio (IFAR) are the same as those for a 1.5-MJ target [Goncharov *et al.*, Phys. Rev. Lett. **104**, 165001 (2010)] designed to ignite on the National Ignition Facility [Hogan *et al.*, Nucl. Fusion **41**, 567 (2001)]. The results from a series of 29 cryogenic DT implosions are presented. The implosions were designed to span a broad region of design space to study target performance as a function of shell stability (adiabat) and implosion velocity. Ablation-front perturbation growth appears to limit target performance at high implosion velocities. Target outer-surface defects associated with contaminant gases in the DT fuel are identified as the dominant perturbation source at the ablation surface; performance degradation is confirmed by 2D hydrodynamic simulations that include these defects. A trend in the value of the Lawson criterion [Betti *et al.*, Phys. Plasmas **17**, 058102 (2010)] for each of the implosions in adiabat–IFAR space suggests the existence of a stability boundary that leads to ablator mixing into the hot spot for the most ignition-equivalent designs. © *2013 AIP Publishing LLC*. [http://dx.doi.org/10.1063/1.4805088]

I. INTRODUCTION

Layered cryogenic deuterium–tritium (DT) capsules are being imploded on the 60-beam OMEGA laser[1] at the Laboratory for Laser Energetics (LLE) to demonstrate hydrodynamic implosion performance equivalent to that of a symmetric direct-drive target designed to ignite with the laser energy available on the National Ignition Facility (NIF).[2] Hydrodynamic equivalence implies that the shell velocity at the end of acceleration (typically referred to as the implosion velocity or V_{imp}), the in-flight aspect ratio (IFAR, defined as the ratio of the shell radius and the shell thickness evaluated after the shell has imploded to 2/3 of its initial radius), and the peak laser drive intensity (I_{L}) are the same as those of a symmetric ignition design[3] for the NIF. The demonstration of direct-drive hydrodynamic equivalence is viewed as an important scientific prerequisite for proceeding with a polar-drive (PD)-ignition campaign on the NIF later in this decade.[4]

The PD concept[5] was developed in 2004 to provide a platform for directly driven implosions on the NIF while the facility is configured for x-ray drive. A preliminary assessment of PD hot-spot target designs has shown that direct-drive ignition might be achieved on the NIF with a laser energy as low as 1 $\mathrm{MJ_{UV}}$.[6] The experimental plan to support the PD-ignition campaign is based on the validation of symmetric direct-drive performance modeling (laser coupling,[7–10] shock timing[11] and thermal transport,[12,13] hot-electron generation,[14] and adiabat control[15]) using cryogenic layered DT implosions on OMEGA. Additionally, select 40-beam, ambient gas-filled PD implosions are being used to confirm drive symmetry modeling.[16] Therefore, PD-ignition designs for the NIF will be based on physics models embedded in the radiation–hydrodynamic design codes that have been validated against symmetric direct-drive-implosion data.

The cryogenic implosion database at the Omega Laser Facility includes over 270 layered fuel implosions (roughly half using pure deuterium D_2 fuel and half using DT). The first cryogenic D_2 capsule implosions[17] were performed in 2000 and cryogenic DT implosions[18] began in

[a)]Paper NI2 2, Bull. Am. Phys. Soc. **57**, 200 (2012).
[b)]Invited speaker.
[c)]Also at Department of Mechanical Engineering, University of Rochester, Rochester, New York 14627, USA.
[d)]Also at Department of Physics and Astronomy, University of Rochester, Rochester, New York 14627, USA.
[e)]Present address: Lawrence Livermore National Laboratory, Livermore, California 94551, USA.
[f)]Also at Department of Chemical Engineering, University of Rochester, Rochester, New York 14627, USA.

late 2006. Among the highlights of these experiments was the demonstration of areal densities in D_2 fuel in excess of 200 mg/cm^2,[12,19] the demonstration of areal densities in DT fuel of 300 mg/cm^2 (Refs. 3 and 20) (nominally the minimum areal density needed to sustain a thermonuclear burn wave), and the demonstration of yields relative to 1D predictions in excess of 15%.[21]

This manuscript describes recent progress toward demonstrating ignition hydrodynamically equivalent implosion performance on OMEGA. The concept of hydrodynamic similarity and the requirements for OMEGA target design are discussed in Sec. II. The data from 29 symmetrically driven cryogenic DT implosions spanning a design space that includes ignition are shown in Sec. III. A discussion of the data in this section concludes that target performance on OMEGA is impacted by capsule surface perturbations, leading to ablator mixing into the hot spot. The origin and hydrodynamic modeling of these capsule surface perturbations are discussed in Sec. IV. In Sec. V, all of the cryogenic DT data are plotted using the experimental ignition threshold factor (ITFx) formalism described in Ref. 22 scaled appropriately for the target mass and laser energy differences between OMEGA and the NIF. The ITFx formalism is a convenient metric for comparing relative target performance across a broad design space and is related to the generalized Lawson criterion applied to inertial confinement fusion (ICF) derived by Zhou and Betti[23] Concluding remarks are given in Sec. VI.

II. HYDRODYNAMIC SIMILARITY AND EXPERIMENTAL DESIGN

Hydrodynamic similarity can be used to extrapolate implosion performance from the 26-kJ$_{UV}$ OMEGA to the 1.8-MJ$_{UV}$ NIF laser. In this way, implosions can be performed on OMEGA to probe the design space for targets on the NIF. In Ref. 24, Betti *et al.* showed explicitly that an ignition design for the NIF based on a specific adiabat (α, defined as the ratio of the shell pressure to the Fermi degenerate pressure), implosion velocity, and laser intensity can be reproduced on OMEGA with the same adiabat, implosion velocity, and laser intensity. While this scaling should lead to the same peak stagnation pressure and density in the OMEGA and NIF cores, the resulting yields and fuel areal density will necessarily be lower on OMEGA because of the smaller fuel mass and laser energy. Indeed, for hydrodynamic similarity, the target mass scales as the laser energy E_L, the target radius as $E_L^{1/3}$, the laser power as $E_L^{2/3}$, and the laser pulse length as $E_L^{1/3}$.

The assumption implicit in the hydro scaling argument is that the ablation pressure and preheat sources are independent of target scale (and facility). This is unlikely to be the case, however, since the coronal plasma scale length on the NIF relative to OMEGA will scale as the radius of the capsule (approximately 4× longer) for hydrodynamically similar implosions. The longer plasma scale lengths will reduce the ablation pressure via light-scattering losses and increased cross-beam energy transfer (CBET)[8] and will increase the production of hot electrons (and potentially fuel preheating) from the two-plasmon-decay (TPD) instability.[14,25] Although these laser–plasma instabilities do not *a priori* restrict the design space available on OMEGA for ignition-relevant implosions, they may limit the ultimate performance that can be achieved.

The cryogenic target design for the experiments discussed in this manuscript is shown in Fig. 1. This design is scaled from the 1.5-MJ symmetric direct-drive–ignition design published by Goncharov *et al.*[3] The capsule ablator material [Fig. 1(a)] is pure CD or CD doped with a few atomic percent of silicon (the dopant tailors the adiabat at the ablation surface to reduce the imprint growth rate[7]). The peak intensity of the triple-picket drive pulse [Fig. 1(b)] is 9×10^{14} W/cm^2; the total drive energy is designed to be 25 kJ. The capsule radius is nominally 430 μm, which is $(1.5\text{ MJ}/0.025\text{ MJ})^{1/3} \sim 3.9\times$ smaller than the 1.5-MJ ignition design (1700 μm).

Based on the hydrodynamic similarity argument above, this target platform can be used to access a broad region of design space that includes the 1.5-MJ ignition design. With constant drive intensity and laser energy, the V_{imp} and IFAR are varied by changing the thickness of the ablator and DT ice layer and adjusting the picket energies and temporal spacing to achieve the desired adiabat at the inner fuel surface (the picket adjustments are used to ensure the correct shock timing and radial convergence). Figure 2 is a scatter plot in IFAR and adiabat space of 29 layered cryogenic DT capsule implosions on OMEGA (i.e., each point represents an implosion on OMEGA with the indicated adiabat and IFAR). These implosions are selected from a set of nearly 60 experiments (performed over the past 18 months) based on a set of "physics quality" criteria that include target alignment at shot time (within 15 μm of target chamber center), ice layer quality (less than 2-μm rms over all modes), and pulse-shape quality (typically picket energies within 10% of the design specification). The shaded region for IFAR > 23 shows the approximate design space for ignition with implosion velocities between 350 and 400 km/s.

Figure 1(a) shows the range of ablator and ice thickness used for the points shown in Fig. 2. The implosion velocities range from 250 km/s to 380 km/s (e.g., a 9.2-μm CD ablator with an ice layer of 48 μm is predicted to achieve a V_{imp} of 350 km/s). Although the adiabat, IFAR, and V_{imp} are calculated quantities (based on the 1D design code *LILAC*[26]), the

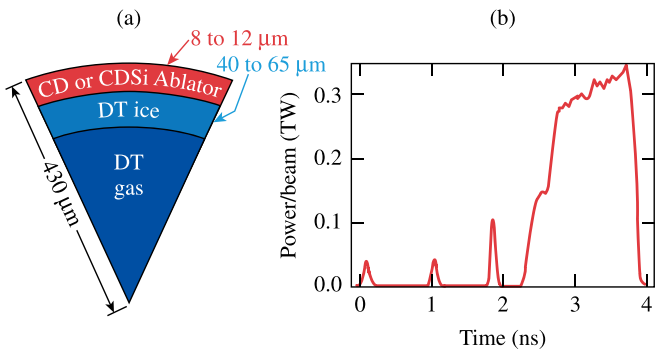

FIG. 1. (a) The standard cryogenic DT capsule imploded on OMEGA consists of a thin CD or doped-CD ablator fill with several hundred atm of DT gas to create a 40- to 60-μm-thick ice layer. (b) The standard 25-kJ drive pulse consists of a series of three pickets used to establish the shell adiabat and control shock coalescence and a high-intensity main drive.

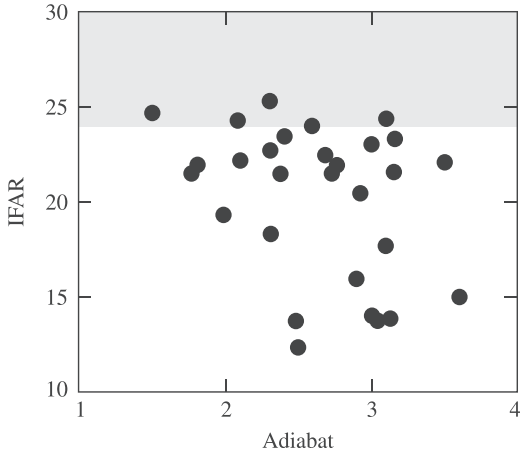

FIG. 2. A scatter plot in IFAR–adiabat design space of 29 cryogenic DT implosions on OMEGA. Each black circle represents an implosion with the specific post-shot calculated values of IFAR and adiabat. The shaded region represents the ignition-relevant region of this design space.

V_{imp} is confirmed experimentally by measuring the implosion burn history using the neutron temporal diagnostic (NTD).[27] *LILAC* incorporates nonlocal thermal transport[12] and a stimulated Brillouin scattering (SBS) model[8] to account for cross-beam energy transfer. A 10% change in the predicted velocity is a timing shift of 150 ps in the NTD. The absolute temporal accuracy of the NTD is 25 ps so the implosion velocity is known to within a few percent.

III. MEASUREMENTS AND DISCUSSION

The ICF Lawson criterion[23] can be used to connect the design parameters (V_{imp}, adiabat, and IFAR) to the experimentally measured observables. These observables include the primary neutron yield Y_n, the compressed fuel areal density ρR, the hot-spot ion temperature T_{ion}, the absorbed laser energy, and the neutron burn history. The Lawson criterion is defined as $\chi = P\tau/P\tau(T)_{ign} > 1$,[28] where P is the plasma pressure and τ is the energy confinement time. In Ref. 28, Betti *et al.* derived an approximate 1D ignition parameter based on the generalized Lawson criterion

$$\chi(1D) \sim (\rho R^{no\,\alpha})^{0.8} \times (T_{ion}^{no\,\alpha}/4.4)^{1.8} > 1, \qquad (1)$$

where T_{ion} is given in keV and ρR in g/cm^2. The superscript "no α" indicates that alpha-particle-energy deposition is turned off in the 1D simulations used to validate the analytic scaling. Recognizing that implosion nonuniformities significantly degrade 1D performance, the authors used a simple 3D burn model to derive a generalized Lawson criterion

$$\chi(3D) \sim (\rho R^{no\,\alpha})^{0.8} \times (T_{ion}^{no\,\alpha}/4.4)^{1.8} \times YOC_{3D}^{m}. \qquad (2)$$

YOC_{3D} (yield-over-clean) is the ratio of the estimated 3D yield to the predicted 1D yield and m is analytically given as 0.64 but is between 0.4 and 0.5 based on fitting simulation yields with an ignition criterion of $\chi \sim 1$. It is difficult to use this form of χ to evaluate absolute implosion performance given the dependence on simulations and the measured T_{ion}, which is sensitive to fuel motion. Therefore, Betti *et al.*[24] modified Eq. (2) to remove the explicit dependence on the YOC parameter and replace the T_{ion} with the absolute yield Y_n. This version of the "measurable" generalized Lawson criterion for ICF is given by

$$\chi \sim (\rho R^{no\,\alpha})^{0.61} \times (0.24\,Y_n/M_{fuel})^{0.34}, \qquad (3)$$

where ρR is in g/cm^2, Y_n is in units of 10^{16}, and M_{fuel} is in mg. This form of χ depends only on the measured fuel ρR and the neutron yield and is roughly equivalent to the cube root of the ITFx derived by Haan *et al.*[22]

It can be shown[24] that ignition hydrodynamically equivalent implosions on OMEGA occur for values of $\chi > 0.16$. This can be satisfied for a range of areal densities and yields. Given that a ρR of $\sim$300 mg/cm^2 has already been demonstrated on OMEGA,[3,20] a $\chi \sim 0.16$ corresponds to a yield of 4×10^{13}. These values of Y_n and ρR provide a convenient metric for demonstrating ignition hydrodynamically equivalent implosion performance with symmetric direct drive on OMEGA and are consistent with an earlier analysis discussed in Ref. 20.

Figure 3 shows the dependence of the 1D fractional measured ρR ($\rho R/\rho R_{1D}$) as a function of the calculated fuel adiabat [Fig. 3(a)] and IFAR [Fig. 3(b)] for the 29-shot database shown in Fig. 2. As expected, the fraction of the 1D ρR produced in the implosions is lower for higher-convergence, lower-adiabat implosions. The trend of lower ρR with decreasing shell stability is also clear as a function of IFAR. The measured fraction of the 1D ρR approaches 80% for values of the adiabat above $\sim$2.5 and for values of IFAR below $\sim$20. Burn truncation[29] and ^{3}He buildup in the capsule due to tritium β-decay can account for much of the degradation relative to the prediction. Estimates of the void pressure caused by the buildup of ^{3}He are sufficient to cause a degradation of the predicted ρR of 10% to 15%. The 1D prediction for the points in Fig. 3 does not take into account the increased pressure in the capsule caused by ^{3}He buildup as the target ages.

The ρR measurements in Fig. 3 were obtained with two independent instruments: the magnetic recoil spectrometer (MRS)[30] and a highly collimated neutron time-of-flight

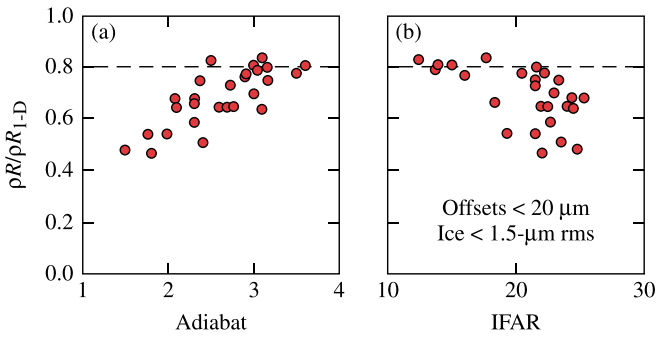

FIG. 3. (a) The correlation between the ratio of the measured and 1D-predicted areal density and the calculated adiabat for the implosions in Fig. 2 shows a drop in the measured ρR for adiabats generally less than 2.5. (b) The correlation between the ratio of the measured and 1D-predicted areal density and the calculated IFAR for the implosions in Fig. 2 shows a drop in the measured ρR for IFARs generally greater than 17.

(nTOF) detector.[31] The areal density inferred from the nTOF is based on a different part of the (n,T) scattering cross section[32] than used in the reduction of the MRS data. While the MRS measures the fraction of the primary yield forward scattered by the compressed DT, the nTOF measures the (n,T) backscatter edge at 3.5 MeV to infer the triton density in the compressed fuel. The systematic error on the ρR inferred from the nTOF is somewhat higher (estimated to be $<15\%$) than that from the MRS (6%). However, where both measurements are available (a small number of the experiments did not have the nTOF available), the value of the ρR used in Fig. 3 is the average of the two measurements.

Figure 4 is a duplicate of Fig. 2 with contours of constant $\rho R/\rho R_{1D}$ for the 29 experiments. In this 2D design space, a stability boundary suggested by Figs. 3(a) and 3(b) is clearly evident. For this set of experiments, the edge of the boundary can be roughly defined as $\text{IFAR} = 20(\alpha/3)^{0.8}$. While Fig. 3(b) suggests that the measured ρR begins to deviate from the 1D prediction for values of IFAR > 17, the 2D contour plot clearly shows that the 1D ρR is recovered for larger IFAR as long as the adiabat is suitably large. This further confirms that the stability of these targets is sensitive to design details that can be fully accessed based on the flexibility of the target platform.

Figure 5 shows the measured (red circles) and 1D predicted (black circles) Y_n [Fig. 5(a)] and T_{ion} [Fig. 5(b)] as a function of the calculated implosion velocity. The measured yield increases uniformly with implosion velocity from 250 km/s to 380 km/s. The larger spread in the experimental yields for $V_{imp} \sim 300$ to 320 km/s suggests that the shell is becoming increasingly unstable as the implosion velocity is increased. The data points at higher V_{imp} were therefore acquired using a higher fuel adiabat to stabilize perturbation growth at the ablation surface and the ice–gas interface. This additional stabilization is clearly evident in Fig. 5(b), where there is little variation in the measured T_{ion} with increasing V_{imp} until the fuel adiabat is raised to access V_{imp} above ~320 km/s. With the higher-adiabat implosions, T_{ion} increases rapidly with V_{imp} reaching 90% to 95% of the prediction at 380 km/s.

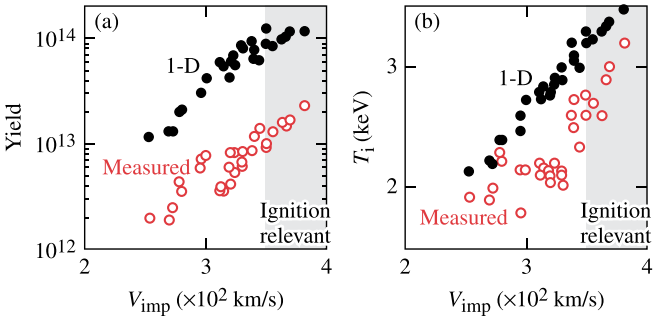

FIG. 5. (a) The 1D and measured yields increase with increasing implosion velocity. The adiabat was increased to reach implosion velocities above 330 km/s. (b) While the 1D ion temperature increases linearly with the implosion velocity, the measured temperature is fairly constant until the implosion velocity exceeds 330 km/s. The shaded regions indicate ignition-relevant implosion velocities.

Figure 6 is a duplicate of Fig. 2 with contours of constant $Y_n/Y_{n\,1D}$ [this is the ratio of the measured and simulated yields from Fig. 5(a), commonly referred to as YOC] across the 29 experiments. The vertical contours indicate that the measured yield depends primarily on the adiabat for values of IFAR < 20 to 22. Only at the highest adiabat does the yield appear to be independent of IFAR for ignition-relevant values (a target is unlikely to ignite at these adiabats with the energy available on the NIF). The YOC for these few data points is >20%. The YOC for ignition-relevant values of the adiabat and IFAR is generally less than 10%.

The largest value of χ [Eq. (3)] in this data set is 0.09. For this shot (and several others in the 0.08 range), the value of the measured ρR and Y_n are approximately half of the values needed to demonstrate ignition hydrodynamically equivalent implosion performance. These highest-performing implosions are not associated with ignition-relevant values of IFAR and adiabat. This is seen in Fig. 7 where contours of constant χ/χ_{1D} are plotted in the IFAR–adiabat space of Fig. 2 across the 29-point experimental database. The contours clearly show that relative to 1D prediction, target performance decreases with increasing IFAR and decreasing adiabat. Not surprisingly, this is consistent with the stability boundary identified in Fig. 4.

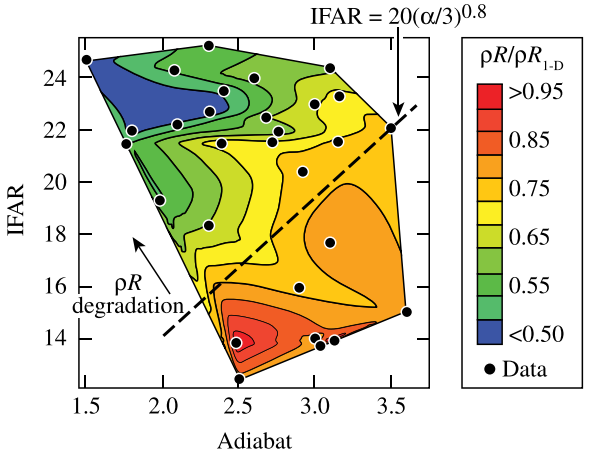

FIG. 4. Contours of the measured areal-density fraction relative to 1D prediction ($\rho R/\rho R_{1D}$) show a steep drop for values of the IFAR above the line defined by $20(\alpha/3)^{0.8}$.

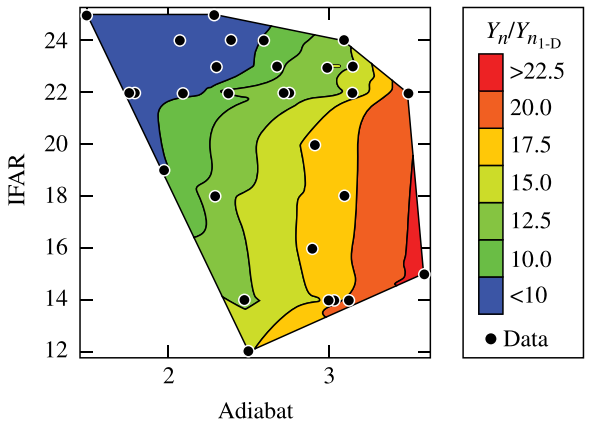

FIG. 6. Contours of the measured yield fraction relative to 1D predictions (YOC) show that the yield depends primarily on the adiabat for IFARs generally less than 20.

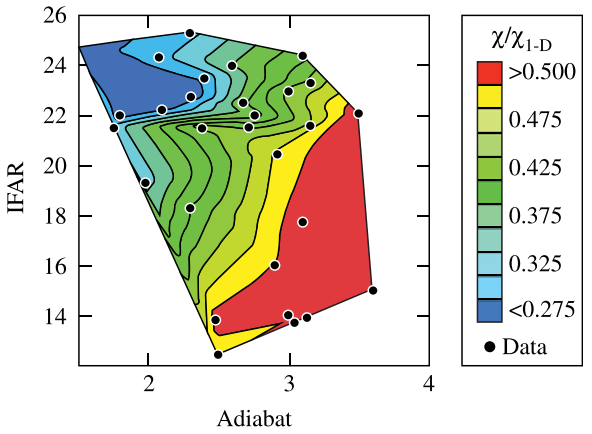

FIG. 7. Contours of the measured χ fraction relative to the 1D-predicted χ show a steep drop with increasing IFAR for ignition-relevant adiabats (<2.5).

Together, these data suggest that as the design approaches ignition hydrodynamic equivalence, the fuel shell breaks apart during acceleration, leading to a drop in the burn-averaged fuel areal density. The subsequent loss in the hot-spot pressure and temperature leads to a drop in the primary yield. The shell breakup during acceleration suggests Rayleigh–Taylor (RT) perturbation growth from the ablation surface (as opposed to deceleration driven growth at the ice–-gas interface). Such growth would be expected to mix ablator material in the core. This mixing is confirmed in Fig. 8, where the yield-normalized x-ray emission from the core is plotted as a function of the adiabat. The yield normalization factor comes from a fit of the 1D-predicted x-ray emission. When normalized to $Y_{1D}^{0.57}$, simulated core x-ray emission is approximately constant for all of the experiments. This is shown by the black circles in Fig. 8. If carbon mixing enhances the core emission, this should be evident when the experimental x-ray emission is normalized to $Y_{\text{measured}}^{0.57}$. These values are plotted as red squares. The data clearly show that

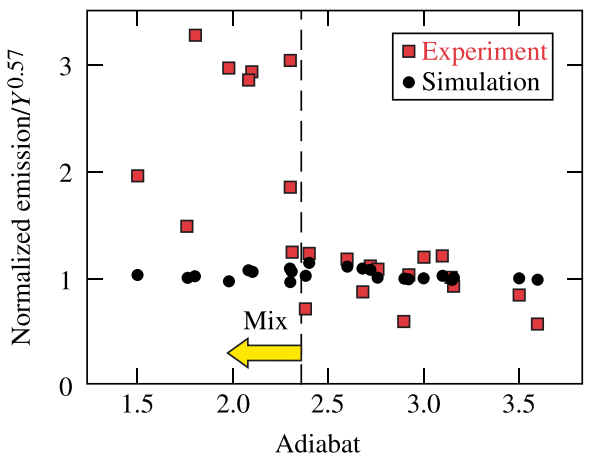

FIG. 8. The yield normalized x-ray emission from 1D simulations (black circles) and cryogenic DT implosions (red boxes) is plotted as a function of the implosion adiabat. The experimental points show a pronounced increase in the x-ray emission relative to 1D prediction for adiabats generally less than 2.5, indicating that this emission is caused by higher-Z carbon mixing into the core.

when the adiabat is less than 2.5, the core x-ray emission is strongly enhanced relative to the high-adiabat experiments where Figs. 4 and 6 show that the shell is likely integral through acceleration. The normalization of the experimental and simulated points at high adiabats is arbitrary as are the units of the normalized emission. The simulated x-ray emission used to establish the yield normalization is restricted to the sensitivity range of the gated x-ray imager used for the measurement (roughly 4–7 keV).

IV. CAPSULE SURFACE QUALITY AND 2D SIMULATIONS

As discussed in Sec. III, the accumulated data suggest a high level of ablator mixing into the hot spot at peak burn. This level of mix would require a significant source of perturbations on the capsule surface to drive CD into the core before stagnation. The shadowgraphy-based imaging system used to characterize the ice layer quality was refocused to image the capsule surface. Figure 9 shows a stitched image in pixel space of five capsule surface images acquired at the same focal depth as the target was rotated. The stitched image contains about 2/3 of the capsule surface and shows dozens of surface "defects" distributed randomly (there is no discernible pattern from one target to another) across the surface.

A detailed optical analysis of these defects confirms that most of the features reside on the outer capsule surface and originate during the high-pressure fill and cooling cycle (Ref. 18 describes the permeation filling process and the DT layering/characterization in detail), i.e., the features do not correspond with fabrication defects identified prior to the fill. A subset of the filled capsules has a small number of dendritic defects on the inner surface of the CD shell. An analysis of one of these inner-surface dendritic defects following a controlled depressurization of a filled capsule showed that the radial depth is of the order of 0.1 μm or less, within the smoothness specification for the capsule.

Every target imploded on OMEGA since January 2012 has had the surface defects analyzed based on images such as the one shown in Fig. 9. The analysis identifies the type of defect (outer surface or inner surface) and the defect area. Figure 10(a) is a plot of the defect-size distribution for the targets filled in 2012 (48 total). The average defect size is

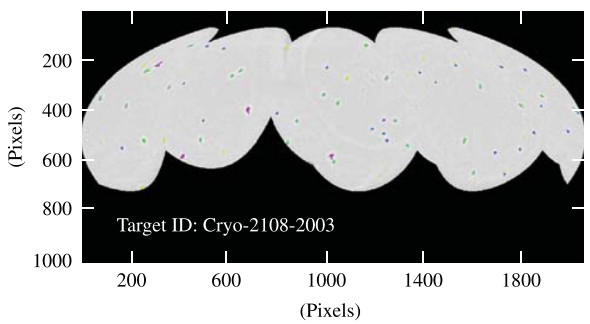

FIG. 9. A stitched set images of the cryogenic DT capsule surface during characterization. The image shows dozens of surface defects associated with the high-pressure DT permeation fill. The defects are likely frozen gas contaminants in the DT fuel.

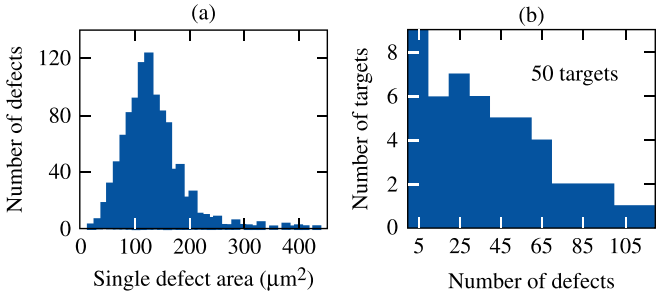

FIG. 10. (a) The defect-size distribution for the targets characterized in 2012 shows that the average defect size is about 140 μm^2. (b) The frequency distribution of the defects on 50 targets filled and characterized in 2012. Most targets have several dozen individual defects.

around 140 μm^2; the imaging system is capable of resolving features with an area as small as 20 μm^2. Figure 10(b) shows a histogram of the target defect frequency distribution (bin size is ten defects). The defect count can exceed 100 on a single target. The total defect area for the 29 targets discussed in this paper ranged from a few thousand up to 15 000 μm^2 (nearly 1% of the total capsule surface area). The variation in defect count and total area from target to target and fill to fill is not understood.

Two-dimensional simulations of a single isolated surface defect suggest that the defects account for much of the observed target performance degradation relative to 1D prediction. The implosion performance of several targets was simulated by assuming a uniform distribution of constant-size defects (80 μm^2) with a thickness of 1 μm. The thickness of the defects cannot be measured with the optical imaging system used to characterize the DT ice layer (limited spatial resolution and contrast) unless they can be resolved on the limb of the images. In some cases, this has been possible; however, most of the defects cannot be identified on the limb of the capsule images. A thickness of 1 μm was used in the simulations as a compromise—some will be larger while most are smaller. A 2D simulation with a single defect and reflecting boundary conditions was performed using a sector defined as $4\pi/N$, where N is the number of defects on the target. The reflecting boundaries mimic the presence of neighboring defects in this simplified 2D simulation. Assuming that the defects are identical and uniformly distributed around a target, the predicted yield is then N times the results of the simulation. The simulated ion temperature and neutron averaged ρR are taken as the average for the target. Table I shows the results of these simulations for shot 66999 (August 2012).

TABLE I. For shot 66999, the results of 1D simulations including nonlocal thermal transport and cross-beam energy transfer, 2D simulations with imprint, and 2D simulations based on an isolated surface defect are compared with the measured yield, areal density, and ion temperature.

Shot 66999	Y_n ($\times 10^{13}$)	ρR (mg/cm^2)	T_{ion} (keV)
1D (NL + SBS)	7.9	238	3.1
2D imprint	4.5	242	3.4
2D defect	1.8	151	2.7
Measured	1.2	175	2.5

The first row is the 1D prediction using *LILAC* with nonlocal thermal transport and a SBS model to account for cross-beam energy transfer in the absorbed energy.[8] The second row is the 2D simulation described above including single-beam laser imprint[33] but no isolated defects. The third row is the 2D simulation including the average isolated defect with $N = 150$. The fourth row is the experimentally measured values. The isolated defect simulation reproduces the experimental measurements reasonably well, while the imprint-only simulations cannot explain the observed implosion performance. The other simulated implosions show a quantitatively similar behavior with respect to measured target performance. While the number of defects simulated was larger than the average number shown in Fig. 10(b) and the area of each defect was less than the average shown in Fig. 10(a), the total defect area was similar to the average of most targets in the 2012 database. The key point is that injecting the proper amount of ablator material into the core via ablation-front RT growth reproduces the experimental performance observables.

Further progress toward the demonstration of ignition hydrodynamically equivalent implosion performance requires that these isolated defects be eliminated from the capsules. Few, if any, of these defects are particulate in nature. Steps taken in 2011 eliminated the identified sources for particulate debris. The defects are condensed non-hydrogenic gases entrained in the closed DT fuel supply; analysis confirms that the fuel supply contains nearly 0.5% organics and hundreds of ppm of nitrogen, water, and CO_2. The organics are likely generated by the energetic tritium β-decay electrons that liberate carbon atoms from the CD capsule and the cryogenic epoxies used in the target mounts (the target and support structures are immersed in DT gas during the diffusion fill and the pressure is ramped up to hundreds of atmospheres at room temperature over a 24- to 36-h period).[18] Since the DT fuel supply is operated as a closed loop, organics formed during a fill remain entrained in the fuel for subsequent fills.

The gases condense on the outer surface of the capsule as it is being cooled under pressure. As the temperature of the DT approaches the triple point, the DT liquefies, immersing the capsule and effectively stopping further contaminant gas condensation from the vapor phase on the outer surface. The contaminant gases are presumably on the inside of the capsule as well since the shell is quite permeable at room temperature. The gases likely form monolayers on the inner surface as the temperature falls below the various triple points. Based on the characterization possible to date, there is no visible evidence of crystalline or condensation-related features on the inner surface of the CD shell. Any features on the inner surface would need to first feed out to the ablation surface (where the amplitudes would be quite reduced) to be associated with carbon mixing in the core (recall Fig. 8).

Two facility projects are underway to eliminate these "trace" gases in the fuel supply: The first—a PdAg filter[34] that will pass only hydrogen into the high-pressure permeation cell with the capsules—will be available in early 2013. An isotope separation unit is under development to remove all contaminants from the DT fuel supply including protium (^{1}H). This system is expected to become operational in late 2013.

V. ITFx

The goal of the National Ignition Campaign (NIC) was to demonstrate alpha heating and ignition using indirectly driven (ID) cryogenic DT implosions on the NIF.[35] Using multidimensional hydrodynamic simulations, Haan *et al.*[22] derived a convenient metric (ITFx) for tracking the relative implosion performance as capsule and drive parameters were tuned to achieve the required implosion symmetry, fuel adiabat, and implosion velocity. The ITFx is given by

$$\mathrm{ITFx(ID)} = (Y_\mathrm{n}/3.2\times10^{15})\times(\mathrm{DSR}/0.07)^{2.3}, \quad (4)$$

where DSR is the "down-scatter ratio"[36] in percent and related[37] to the total fuel areal density by ρR (g/cm^2) $=21\times$ DSR (%), i.e., the normalization factor of 0.07 is effectively a fuel areal density of 1.5 g/cm^2. The normalization factors on the yield and areal density are set so that an ITFx of unity implies a 50% probability that the target would ignite (given the spectrum of tolerances used in the simulations). Symmetric DD implosions on OMEGA can be plotted using the ITFx(ID) on an equivalent performance basis by using the standard hydrodynamic scaling relations[24] $\rho R\sim E_\mathrm{L}^{1/3}$, $Y\sim T_\mathrm{i}^{4.7}\times\rho\mathrm{R}^{0.56}\times M_\mathrm{fuel}$, and $T\sim E^{0.07}$. The ignition Y_n and ρR in Eq. (4) can be replaced by laser energy and mass-scaled quantities from OMEGA cryogenic DT implosions. The OMEGA ignition equivalent ITFx is then

$$\mathrm{ITFx(NIF\,DD)} = \mathrm{ITFx(ID\,\Omega)}\times(E_\mathrm{NIF}/E_\Omega)^{1.28}\times(M_\mathrm{NIF}/M_\Omega)\times(\mathrm{YOC_{NIF}}/\mathrm{YOC_\Omega}), \quad (5)$$

where ITFx (ID Ω) is Eq. (4) with the OMEGA (Ω) measured quantities, E is the laser energy, M is the fuel mass, and YOC is based on an equivalent perturbation spectrum for each facility.[24] The assumption is that the YOC on the NIF will be higher than on OMEGA for an equivalent perturbation spectrum given the larger capsule and consequent smaller perturbation wavelengths. For $E_\mathrm{NIF}=1.8$ MJ, $E_\Omega=25$ kJ, $M_\mathrm{NIF}=0.17$ mg, $M_\Omega=0.02$ mg, $\mathrm{YOC_{NIF}}=50\%$, and $\mathrm{YOC_\Omega}=25\%$ (best $\mathrm{YOC_\Omega}$ for an adiabat of ~3 and V_imp of ~350 km/s)

$$\mathrm{ITFx(NIF\,DD)} = 3505\times\mathrm{ITFx(ID\,\Omega)}. \quad (6)$$

Figure 11 shows the distribution of the scaled ITFx (NIF DD) for the 29 implosions discussed above in a plot of measured yield and ρR. The blue squares are pure CD ablators, while the orange diamonds are Si-doped ablators (typically a few atomic % of silicon in the outer few microns of the shell). The red circles are from a high areal density series of experiments performed in 2009.[3,20] There is no discernible difference between the doped and undoped ablators, confirming the conclusion from Table I that imprint cannot explain the current target performance. Curves of constant ITFx(NIF DD) from Eq. (6) are superimposed along with data points from a high-ρR series of implosions in 2009.[3,20] The best-performing implosions on OMEGA have achieved an equivalent NIF direct-drive ITFx of nearly 0.2. The highest ρR to date in an OMEGA DT implosion (~295 mg/cm^2) produced

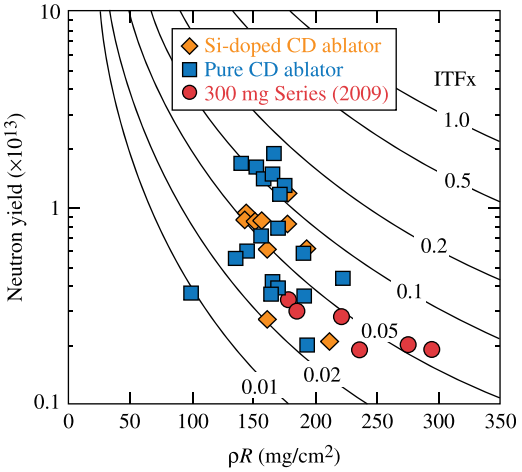

FIG. 11. The 29 implosions represented in Fig. 2 are plotted according to the measured yield and areal density. Curves of constant NIF-equivalent direct-drive ITFx [Eq. (6)] are also plotted. The blue squares are pure CD ablators while the orange diamonds are Si-doped ablators. The red circles are from a high areal density series of experiments performed in 2009.[3,20]

an ITFx (NIF DD) of nearly 3× less due to the low yield. An ITFx (NIF DD) of unity is satisfied for an areal density of 300 mg/cm^2 and a yield of 3×10^{13}, very similar to the values derived by Betti *et al.*[24] from the generalized Lawson criterion for ICF and discussed above.

VI. CONCLUSION

The goal of the cryogenic DT implosion experiments at LLE is to demonstrate ignition hydrodynamic similarity. In little more than a year, cryogenic DT implosions on OMEGA have probed a broad region of design space that includes fuel adiabats from <2 to nearly 4, IFARs from <15 to more than 25, and implosion velocities from 250 to 380 km/s. Several of the targets would have demonstrated ignition hydrodynamic equivalence had the measured performance agreed with the 1D prediction. The key to this rapid progress is the flexible, symmetric direct-drive target platform on the OMEGA laser. With the peak drive intensity defined by the hydro scaling discussed in Sec. II, the adiabat on any layered DT target can be easily changed by adjusting the laser drive picket energies and relative timings while the implosion velocity and IFAR are set by the mass of the ablator and ice.

The conclusion from the data and 2D simulations is that the stability of the imploding shell is compromised by dozens of isolated outer surface defects. These defects act as perturbation seeds that grow rapidly at the ablation surface and mix ablator material into the core. The defects appear on the capsules following the permeation fill process and are most likely caused by contaminant gases in the DT fuel supply that freeze on the surface of the capsule as it is being cooled under pressure. Defect-free targets are expected within a few months once the DT fuel is purified (the first step is the use of a palladium–silver filter to remove the non-hydrogen contaminants reaching the capsules; this will be followed later in 2013 with an isotope separation capability that will remove all of the contaminants including ^{1}H).

High implosion velocities are achieved with higher-adiabat target designs that stabilize the defect growth at the ablation surface. At the highest adiabats, the measured areal density and primary neutron yield are >80% and >20% of the 1D prediction, respectively. Comparable performance relative to 1D at adiabats around 2 is needed to demonstrate ignition hydrodynamic similarity. Two-dimensional simulations of the defect growth show that this is the primary cause of performance degradation. Eliminating the defects is a high priority for LLE and the first targets fielded in 2013 are expected to be defect free (apart from fabrication defects and the intrinsic capsule smoothness achieved during manufacturing). Once free of the isolated surface defects, LLE will perform lower-adiabat implosions (implying higher ρR) with improved shell stability (little or no ablator mix) at high implosion velocity. The goal is to achieve a yield of approximately 4×10^{13} and a DT fuel areal density of $300\,\mathrm{mg/cm^2}$. This will be a $\chi \sim 0.16$ and a scaled ITFx greater than unity.

ACKNOWLEDGMENTS

This work was supported by the U.S. Department of Energy Office of Inertial Confinement Fusion under Cooperative Agreement No. DE-FC52-08NA28302, the University of Rochester, and the New York State Energy Research and Development Authority. The support of DOE does not constitute an endorsement by DOE of the views expressed in this article.

[1]T. R. Boehly, D. L. Brown, R. S. Craxton, R. L. Keck, J. P. Knauer, J. H. Kelly, T. J. Kessler, S. A. Kumpan, S. J. Loucks, S. A. Letzring, F. J. Marshall, R. L. McCrory, S. F. B. Morse, W. Seka, J. M. Soures, and C. P. Verdon, Opt. Commun. **133**, 495 (1997).
[2]W. J. Hogan, E. I. Moses, B. E. Warner, M. S. Sorem, and J. M. Soures, Nucl. Fusion **41**, 567 (2001).
[3]V. N. Goncharov, T. C. Sangster, T. R. Boehly, S. X. Hu, I. V. Igumenshchev, F. J. Marshall, R. L. McCrory, D. D. Meyerhofer, P. B. Radha, W. Seka, S. Skupsky, C. Stoeckl, D. T. Casey, J. A. Frenje, and R. D. Petrasso, Phys. Rev. Lett. **104**, 165001 (2010).
[4]P. B. Radha F. J. Marshall, J. A. Marozas, A. Shvydky, I. Gabalski, T. R. Boehly, T. J. B. Collins, R. S. Craxton, D. H. Edgell, R. Epstein, J. A. Frenje, D. H. Froula, V. N. Goncharov, M. Hohenberger, R. L. McCrory, P. W. McKenty, D. D. Meyerhofer, R. D. Petrasso, T. C. Sangster, and S. Skupsky, Phys. Plasmas **20**, 056306 (2013).
[5]S. Skupsky, J. A. Marozas, R. S. Craxton, R. Betti, T. J. B. Collins, J. A. Delettrez, V. N. Goncharov, P. W. McKenty, P. B. Radha, T. R. Boehly, J. P. Knauer, F. J. Marshall, D. R. Harding, J. D. Kilkenny, D. D. Meyerhofer, T. C. Sangster, and R. L. McCrory, Phys. Plasmas **11**, 2763 (2004).
[6]S. Skupsky, R. S. Craxton, F. J. Marshall, R. Betti, T. J. B. Collins, R. Epstein, V. N. Goncharov, I. V. Igumenshchev, J. A. Marozas, P. W. McKenty, P. B. Radha, J. D. Kilkenny, D. D. Meyerhofer, T. C. Sangster, and R. L. McCrory, J. Phys. IV France **133**, 233 (2006).
[7]S. X. Hu, G. Fiksel, V. N. Goncharov, S. Skupsky, D. D. Meyerhofer, and V. A. Smalyuk, Phys. Rev. Lett. **108**, 195003 (2012).
[8]I. V. Igumenshchev, W. Seka, D. H. Edgell, D. T. Michel, D. H. Froula, V. N. Goncharov, R. S. Craxton, L. Divol, R. Epstein, R. Follett, J. H. Kelly, T. Z. Kosc, A. V. Maximov, R. L. McCrory, D. D. Meyerhofer, P. Michel, J. F. Myatt, T. C. Sangster, A. Shvydky, S. Skupsky, and C. Stoeckl, Phys. Plasmas **19**, 056314 (2012).
[9]S. X. Hu, V. A. Smalyuk, V. N. Goncharov, J. P. Knauer, P. B. Radha, I. V. Igumenshchev, J. A. Marozas, C. Stoeckl, B. Yaakobi, D. Shvarts, T. C. Sangster, P. W. McKenty, D. D. Meyerhofer, S. Skupsky, and R. L. McCrory, Phys. Rev. Lett. **100**, 185003 (2008).
[10]P. B. Radha, C. Stoeckl, V. N. Goncharov, J. A. Delettrez, D. H. Edgell, J. A. Frenje, I. V. Igumenshchev, J. P. Knauer, J. A. Marozas, R. L. McCrory, D. D. Meyerhofer, R. D. Petrasso, S. P. Regan, T. C. Sangster, W. Seka, and S. Skupsky, Phys. Plasmas **18**, 012705 (2011).
[11]T. R. Boehly, V. N. Goncharov, W. Seka, M. A. Barrios, P. M. Celliers, D. G. Hicks, G. W. Collins, S. X. Hu, J. A. Marozas, and D. D. Meyerhofer, Phys. Rev. Lett. **106**, 195005 (2011).
[12]V. N. Goncharov, T. C. Sangster, P. B. Radha, R. Betti, T. R. Boehly, T. J. B. Collins, R. S. Craxton, J. A. Delettrez, R. Epstein, V. Yu. Glebov, S. X. Hu, I. V. Igumenshchev, J. P. Knauer, S. J. Loucks, J. A. Marozas, F. J. Marshall, R. L. McCrory, P. W. McKenty, D. D. Meyerhofer, S. P. Regan, W. Seka, S. Skupsky, V. A. Smalyuk, J. M. Soures, C. Stoeckl, D. Shvarts, J. A. Frenje, R. D. Petrasso, C. K. Li, F. Séguin, W. Manheimer, and D. G. Colombant, Phys. Plasmas **15**, 056310 (2008).
[13]S. X. Hu, V. Smalyuk, V. N. Goncharov, S. Skupsky, T. C. Sangster, D. D. Meyerhofer, and D. Shvarts, Phys. Rev. Lett. **101**, 055002 (2008).
[14]B. Yaakobi, P.-Y. Chang, A. A. Solodov, C. Stoeckl, D. H. Edgell, R. S. Craxton, S. X. Hu, J. F. Myatt, F. J. Marshall, W. Seka, and D. H. Froula, Phys. Plasmas **19**, 012704 (2012).
[15]V. N. Goncharov, J. P. Knauer, P. W. McKenty, P. B. Radha, T. C. Sangster, S. Skupsky, R. Betti, R. L. McCrory, and D. D. Meyerhofer, Phys. Plasmas **10**, 1906 (2003).
[16]P. B. Radha, J. A. Marozas, F. J. Marshall, A. Shvydky, T. J. B. Collins, V. N. Goncharov, R. L. McCrory, P. W. McKenty, D. D. Meyerhofer, T. C. Sangster, and S. Skupsky, Phys. Plasmas **19**, 082704 (2012).
[17]C. Stoeckl, C. Chiritescu, J. A. Delettrez, R. Epstein, V. Yu. Glebov, D. R. Harding, R. L. Keck, S. J. Loucks, L. D. Lund, R. L. McCrory, P. W. McKenty, F. J. Marshall, D. D. Meyerhofer, S. F. B. Morse, S. P. Regan, P. B. Radha, S. Roberts, T. C. Sangster, W. Seka, S. Skupsky, V. A. Smalyuk, C. Sorce, J. M. Soures, R. P. J. Town, J. A. Frenje, C. K. Li, R. D. Petrasso, F. H. Séguin, K. Fletcher, S. Padalino, C. Freeman, N. Izumi, R. Lerche, and T. W. Phillips, Phys. Plasmas **9**, 2195 (2002).
[18]T. C. Sangster, R. Betti, R. S. Craxton, J. A. Delettrez, D. H. Edgell, L. M. Elasky, V. Yu. Glebov, V. N. Goncharov, D. R. Harding, D. Jacobs-Perkins, R. Janezic, R. L. Keck, J. P. Knauer, S. J. Loucks, L. D. Lund, F. J. Marshall, R. L. McCrory, P. W. McKenty, D. D. Meyerhofer, P. B. Radha, S. P. Regan, W. Seka, W. T. Shmayda, S. Skupsky, V. A. Smalyuk, J. M. Soures, C. Stoeckl, B. Yaakobi, J. A. Frenje, C. K. Li, R. D. Petrasso, F. H. Séguin, J. D. Moody, J. A. Atherton, B. D. MacGowan, J. D. Kilkenny, T. P. Bernat, and D. S. Montgomery, Phys. Plasmas **14**, 058101 (2007).
[19]T. C. Sangster, V. N. Goncharov, P. B. Radha, V. A. Smalyuk, R. Betti, R. S. Craxton, J. A. Delettrez, D. H. Edgell, V. Yu. Glebov, D. R. Harding, D. Jacobs-Perkins, J. P. Knauer, F. J. Marshall, R. L. McCrory, P. W. McKenty, D. D. Meyerhofer, S. P. Regan, W. Seka, R. W. Short, S. Skupsky, J. M. Soures, C. Stoeckl, B. Yaakobi, D. Shvarts, J. A. Frenje, C. K. Li, R. D. Petrasso, and F. H. Séguin, Phys. Rev. Lett. **100**, 185006 (2008).
[20]T. C. Sangster, V. N. Goncharov, R. Betti, T. R. Boehly, D. T. Casey, T. J. B. Collins, R. S. Craxton, J. A. Delettrez, D. H. Edgell, R. Epstein, K. A. Fletcher, J. A. Frenje, V. Yu. Glebov, D. R. Harding, S. X. Hu, I. V. Igumenshchev, J. P. Knauer, S. J. Loucks, C. K. Li, J. A. Marozas, F. J. Marshall, R. L. McCrory, P. W. McKenty, D. D. Meyerhofer, P. M. Nilson, S. P. Padalino, R. D. Petrasso, P. B. Radha, S. P. Regan, F. H. Seguin, W. Seka, R. W. Short, D. Shvarts, S. Skupsky, V. A. Smalyuk, J. M. Soures, C. Stoeckl, W. Theobald, and B. Yaakobi, Phys. Plasmas **17**, 056312 (2010).
[21]P. B. Radha, R. Betti, T. R. Boehly, J. A. Delettrez, D. H. Edgell, V. N. Goncharov, I. V. Igumenshchev, J. P. Knauer, J. A. Marozas, F. J. Marshall, R. L. McCrory, D. D. Meyerhofer, S. P. Regan, T. C. Sangster, W. Seka, S. Skupsky, A. A. Solodov, C. Stoeckl, W. Theobald, J. A. Frenje, D. T. Casey, C. K. Li, and R. D. Petrasso, IEEE Trans. Plasma Sci. **39**, 1007 (2011).
[22]S. W. Haan, J. D. Lindl, D. A. Callahan, D. S. Clark, J. D. Salmonson, B. A. Hammel, L. J. Atherton, R. C. Cook, M. J. Edwards, S. Glenzer, A. V. Hamza, S. P. Hatchett, M. C. Herrmann, D. E. Hinkel, D. D. Ho, H. Huang, O. S. Jones, J. Kline, G. Kyrala, O. L. Landen, B. J. MacGowan, M. M. Marinak, D. D. Meyerhofer, J. L. Milovich, K. A. Moreno, E. I. Moses, D. H. Munro, A. Nikroo, R. E. Olson, K. Peterson, S. M. Pollaine, J. E. Ralph, H. F. Robey, B. K. Spears, P. T. Springer, L. J. Suter, C. A. Thomas, R. P. Town, R. Vesey, S. V. Weber, H. L. Wilkens, and D. C. Wilson, Phys. Plasmas **18**, 051001 (2011).
[23]C. D. Zhou and R. Betti, Phys. Plasmas **15**, 102707 (2008).

[24]R. Betti, "Theory of ignition and hydro-equivalence for inertial confinement fusion," paper presented at the 24th IAEA Fusion Energy Conference, San Diego, CA, 8–13 October 2012.
[25]H. A. Baldis and C. J. Walsh, Phys. Fluids **26**, 1364 (1983).
[26]J. Delettrez, R. Epstein, M. C. Richardson, P. A. Jaanimagi, and B. L. Henke, Phys. Rev. A **36**, 3926 (1987).
[27]R. A. Lerche, D. W. Phillion, and G. L. Tietbohl, Rev. Sci. Instrum. **66**, 933 (1995).
[28]R. Betti, P. Y. Chang, B. K. Spears, K. S. Anderson, J. Edwards, M. Fatenejad, J. D. Lindl, R. L. McCrory, R. Nora, and D. Shvarts, Phys. Plasmas **17**, 058102 (2010).
[29]P. B. Radha, T. J. B. Collins, J. A. Delettrez, Y. Elbaz, R. Epstein, V. Yu. Glebov, V. N. Goncharov, R. L. Keck, J. P. Knauer, J. A. Marozas, F. J. Marshall, R. L. McCrory, P. W. McKenty, D. D. Meyerhofer, S. P. Regan, T. C. Sangster, W. Seka, D. Shvarts, S. Skupsky, Y. Srebro, and C. Stoeckl, Phys. Plasmas **12**, 056307 (2005).
[30]J. A. Frenje, K. M. Green, D. G. Hicks, C. K. Li, F. H. Séguin, R. D. Petrasso, T. C. Sangster, T. W. Phillips, V. Yu. Glebov, D. D. Meyerhofer, S. Roberts, J. M. Soures, C. Stoeckl, K. Fletcher, S. Padalino, and R. J. Leeper, Rev. Sci. Instrum. **72**, 854 (2001).
[31]C. J. Forrest, P. B. Radha, V. Yu. Glebov, V. N. Goncharov, J. P. Knauer, A. Pruyne, M. Romanofsky, T. C. Sangster, M. J. Shoup III, C. Stoeckl, D. T. Casey, M. Gatu-Johnson, and S. Gardner, Rev. Sci. Instrum. **83**, 10D919 (2012).
[32]J. A. Frenje, C. K. Li, F. H. Séguin, D. T. Casey, R. D. Petrasso, D. P. McNabb, P. Navratil, S. Quaglioni, T. C. Sangster, V. Yu. Glebov, and D. D. Meyerhofer, Phys. Rev. Lett. **107**, 122502 (2011).
[33]V. A. Smalyuk, V. N. Goncharov, K. S. Anderson, R. Betti, R. S. Craxton, J. A. Delettrez, D. D. Meyerhofer, S. P. Regan, and T. C. Sangster, Phys. Plasmas **14**, 032702 (2007).
[34]H. Amandusson, L.-G. Ekedahl, and H. Dannetun, J. Membr. Sci. **193**, 35 (2001).
[35]J. D. Lindl and E. I. Moses, Phys. Plasmas **18**, 050901 (2011).
[36]J. A. Frenje, D. T. Casey, C. K. Li, J. R. Rygg, F. H. Séguin, R. D. Petrasso, V. Yu. Glebov, D. D. Meyerhofer, T. C. Sangster, S. Hatchett, S. Haan, C. Cerjan, O. Landen, M. Moran, P. Song, D. C. Wilson, and R. J. Leeper, Rev. Sci. Instrum. **79**, 10E502 (2008).
[37]A. J. Mackinnon, J. L. Kline, S. N. Dixit, S. H. Glenzer, M. J. Edwards, D. A. Callahan, N. B. Meezan, S. W. Haan, J. D. Kilkenny, T. Döppner, D. R. Farley, J. D. Moody, J. E. Ralph, B. J. MacGowan, O. L. Landen, H. F. Robey, T. R. Boehly, P. M. Celliers, J. H. Eggert, K. Krauter, G. Frieders, G. F. Ross, D. G. Hicks, R. E. Olson, S. V. Weber, B. K. Spears, J. D. Salmonson, P. Michel, L. Divol, B. Hammel, C. A. Thomas, D. S. Clark, O. S. Jones, P. T. Springer, C. J. Cerjan, G. W. Collins, V. Y. Glebov, J. P. Knauer, C. Sangster, C. Stoeckl, P. McKenty, J. M. McNaney, R. J. Leeper, C. L. Ruiz, G. W. Cooper, A. G. Nelson, G. G. A. Chandler, K. D. Hahn, M. J. Moran, M. B. Schneider, N. E. Palmer, R. M. Bionta, E. P. Hartouni, S. LePape, P. K. Patel, N. Izumi, R. Tommasini, E. J. Bond, J. A. Caggiano, R. Hatarik, G. P. Grim, F. E. Merrill, D. N. Fittinghoff, N. Guler, O. Drury, D. C. Wilson, H. W. Herrmann, W. Stoeffl, D. T. Casey, M. G. Johnson, J. A. Frenje, R. D. Petrasso, A. Zylestra, H. Rinderknecht, D. H. Kalantar, J. M. Dzenitis, P. Di Nicola, D. C. Eder, W. H. Courdin, G. Gururangan, S. C. Burkhart, S. Friedrich, D. L. Blueuel, L. A. Bernstein, M. J. Eckart, D. H. Munro, S. P. Hatchett, A. G. Macphee, D. H. Edgell, D. K. Bradley, P. M. Bell, S. M. Glenn, N. Simanovskaia, M. A. Barrios, R. Benedetti, G. A. Kyrala, R. P. J. Town, E. L. Dewald, J. L. Milovich, K. Widmann, A. S. Moore, G. LaCaille, S. P. Regan, L. J. Suter, B. Felker, R. C. Ashabranner, M. C. Jackson, R. Prasad, M. J. Richardson, T. R. Kohut, P. S. Datte, G. W. Krauter, J. J. Klingman, R. F. Burr, T. A. Land, M. R. Hermann, D. A. Latray, R. L. Saunders, S. Weaver, S. J. Cohen, L. Berzins, S. G. Brass, E. S. Palma, R. R. Lowe-Webb, G. N. McHalle, P. A. Arnold, L. J. Lagin, C. D. Marshall, G. K. Brunton, D. G. Mathisen, R. D. Wood, J. R. Cox, R. B. Ehrlich, K. M. Knittel, M. W. Bowers, R. A. Zacharias, B. K. Young, J. P. Holder, J. R. Kimbrough, T. Ma, K. N. La Fortune, C. C. Widmayer, M. J. Shaw, G. V. Erbert, K. S. Jancaitis, J. M. DiNicola, C. Orth, G. Heestand, R. Kirkwood, C. Haynam, P. J. Wegner, P. K. Whitman, A. Hamza, E. G. Dzenitis, R. J. Wallace, S. D. Bhandarkar, T. G. Parham, R. Dylla-Spears, E. R. Mapoles, B. J. Kozioziemski, J. D. Sater, C. F. Walters, B. J. Haid, J. Fair, A. Nikroo, E. Giraldez, K. Moreno, B. Vanwonterghem, R. L. Kauffman, S. Batha, D. W. Larson, R. J. Fortner, D. H. Schneider, J. D. Lindl, R. W. Patterson, L. J. Atherton, and E. I. Moses, Phys. Rev. Lett. **108**, 215005 (2012).